Phase diagram for the Anderson lattice model

B. H. Bernhard* and C. Lacroix
Laboratoire de Magnétisme Louis Néel, CNRS, Grenoble, France

J. R. Iglesias
Instituto de Física, Universidade Federal do Rio Grande do Sul, Porto Alegre, RS, Brazil

B. Coqblin
Laboratoire de Physique des Solides, Université Paris–Sud, Orsay, France
(Received 16 July 1999)

We study the competition between the Kondo effect and the Ruderman-Kittel-Kasuya-Yosida interaction in the framework of the Anderson lattice model with an extra intersite exchange term. By using an approximation based on an atomic expansion, we obtain, for the symmetric half-filled case, a phase diagram analog to the Doniach diagram for the Kondo lattice. The qualitative and quantitative progress in the description of experimental results for the cerium Kondo compounds with respect to previous approaches is discussed. We also calculate the specific heat which exhibits a two-peak structure as a function of temperature.

I. INTRODUCTION

It is well established that there exists, in cerium compounds at low temperatures, a strong competition between the Kondo effect, which is characterized by a heavy-fermion behavior and tends to demagnetize the system, and the Ruderman-Kittel-Kasuya-Yosida (RKKY) interaction, which tends to yield a magnetic ordering. It results that some cerium Kondo compounds are nonmagnetic and exhibit a heavy-fermion behavior, while other ones order magnetically and have a smaller heavy-fermion character.[1]

The competition between the Kondo effect and the RKKY interaction has been described by the Doniach diagram,[2] which gives the Néel and Kondo temperatures as a function of the intrasite exchange constant J_K: the Néel temperature is first increasing with $|J_K|$, then passing through a maximum and reaching zero at a quantum critical point, while the Kondo temperature T_{K0} is exponentially increasing in the single impurity Kondo model. The parameter $|J_K|$ increases with applied pressure or varies with the relative concentration in ternary systems. Such behavior of the Néel temperature has been experimentally observed with increasing pressure in several cerium Kondo compounds, but the Kondo temperature of a compound can be smaller than that predicted by the Doniach diagram.[3]

The Kondo lattice has been studied in a model[3] with both intrasite (J_K) and intersite magnetic exchange interaction (characterized by a nearest-neighbor exchange constant J_H) by means of a mean-field approximation. For sufficiently large intersite antiferrromagnetic correlations, this model yields a decrease of the Kondo temperature as compared to the one-impurity value, giving, therefore, a ''revisited'' version of the Doniach diagram with a rather flat Kondo temperature T_K in the nonmagnetic case, as observed in several cerium compounds. But the two parameters J_K and J_H cannot be considered as independent from each other and it is necessary to take into account the relationship between them to obtain the real dependence of T_K versus J_K. Since the intersite f-f interaction term J_H comes mostly from the indirect RKKY interaction, the value of J_H has been taken proportional to J_K^2. Strong antiferromagnetic short-range correlations decrease drastically the Kondo temperature with respect to that defined for one impurity and can yield roughly constant values of T_K versus J_K. This point is in good agreement with experimental results in $CeRh_2Si_2$ (Ref. 4) where the Kondo temperature T_K is roughly constant with pressure up to 17 kbar and in $CeRu_2Ge_2$ (Refs. 5,6) where T_K increases much less rapidly with pressure than the single impurity Kondo temperature T_{K0} above the critical pressure of supression of the magnetic order. A similar behavior can be found when the relative concentration is varied in a ternary alloy such as $Ce(Ru_{1-x}Rh_x)_2Si_2$.[7,8] Such drastic reduction of the Kondo temperature in a lattice with respect to the one-impurity value has been also obtained by considering the ''exhaustion'' problem due to the fact that only the conduction electrons within an energy range of order T_{K0} from the Fermi energy are able to screen the localized electrons in the Kondo lattice.[9]

In the present paper, we adopt an alternative point of view and, instead of the Kondo Hamiltonian, we consider the periodic Anderson model (PAM), which can describe both Kondo and intermediate valence Cerium compounds. Then, we perform the exact diagonalization of the on-site Hamiltonian, as previously used for the Anderson lattice[10] and the Hubbard Hamiltonians,[11] and we treat the intersite terms within the same preceding diagrammatic approximation. The parameters of this PAM Hamiltonian include the hybridization V, the f-electron energy E_f, and the local Coulomb repulsion U between the f electrons. It corresponds to the Kondo lattice model in the limit $V/|E_f| \to 0$, where the physics is well described by an intrasite exchange constant[12]

$$J_K = \frac{2V^2U}{E_f(E_f+U)}. \tag{1}$$

Thus, based on the results of Ref. 3, we include an extra nearest-neighbor Heisenberg term in order to see the effect of intersite magnetic correlations. In the next section, we present our model Hamiltonian and the approximation adopted that takes into account the strong local correlation between the *f* electrons in a simplified way. In the third section, we present the theoretical results and the comparison with experiments. Then, in the last section, we present some comments and the conclusion.

II. THE THEORETICAL MODEL

The periodic Anderson model (PAM) including nearest-neighbor exchange interactions is described by the following Hamiltonian:

$$\mathcal{H}=\mathcal{H}_0+\mathcal{H}_1+\mathcal{H}_2, \tag{2}$$

where

$$\mathcal{H}_0=\sum_{i\sigma}\left\{E_f n^f_{i\sigma}+\frac{1}{2}U\, n^f_{i\sigma}n^f_{i\bar{\sigma}}+V(f^\dagger_{i\sigma}d_{i\sigma}+\text{H.c.})\right\}, \tag{3}$$

$$\mathcal{H}_1=-\sum_{ij\sigma}\, t_{ij}d^\dagger_{i\sigma}d_{j\sigma}, \tag{4}$$

$$\mathcal{H}_2=-\sum_{ij}\, J_{ij}\mathbf{S}^f_i\cdot\mathbf{S}^f_j, \tag{5}$$

where $a^\dagger_{i\sigma}(a_{i\sigma})$ is the operator that creates (annihilates) one electron of spin σ in the $a=d$ or f orbital at the ith site, $n^a=a^\dagger_{i\sigma}a_{i\sigma}$ is the number operator in that orbital, and $\mathbf{S}^f_i$ is the *f*-electron spin at that site. The parameters included in the first term are the energy E_f of the $4f$ electrons, the Coulomb repulsion U between two f electrons of opposite spin on the same site, and the local hybridization V between f and d electrons. The conduction-electron hopping t_{ij} and the intersite exchange J_{ij} between *f*-electron spins have been considered only for nearest-neighbor sites, in which case they assume the values t and J_H, respectively. Here we consider the symmetric case $(2E_f+U=0)$ at half-filling (two electrons per site), where the chemical potential is equal to zero.

The approximation that we adopt consists of two steps. First, we transform the exchange term $\mathcal{H}_2$ into a one-particle term by applying a mean-field approximation

$$\begin{aligned}\mathbf{S}^f_i\cdot\mathbf{S}^f_j\approx&-\frac{1}{2}\sum_\sigma\,(\langle f^\dagger_{i\sigma}\overrightarrow{f_{j\sigma}}\rangle f^\dagger_{j\sigma}f_{i\sigma}+\langle f^\dagger_{j\sigma}\overrightarrow{f_{i\sigma}}\rangle f^\dagger_{i\sigma}f_{j\sigma}\\&-\langle f^\dagger_{i\sigma}\overrightarrow{f_{j\sigma}}\rangle\langle f^\dagger_{j\sigma}f_{i\sigma}\rangle)-\frac{1}{4}m_im_j\\&+\frac{1}{4}[m_i(n^f_{j\uparrow}-n^f_{j\downarrow})+m_j(n^f_{i\uparrow}-n^f_{i\downarrow})],\end{aligned} \tag{6}$$

where $m_i=\langle n^f_{i\uparrow}\rangle-\langle n^f_{i\downarrow}\rangle$ is the magnetization at the ith site. In this paper we will be restricted to the nonmagnetic phase, where $m_i=0$ and $\langle f^\dagger_{i\sigma}\overrightarrow{f_{j\sigma}}\rangle=\langle f^\dagger_{i\sigma}f_{j\sigma}\rangle=\langle f^\dagger_{j\sigma}f_{i\sigma}\rangle$. In this case, we have

$$\mathcal{H}'_2=-t'\sum_{\langle ij\rangle\sigma}(f^\dagger_{i\sigma}f_{j\sigma}+\text{H.c.})-J_H\sum_{\langle ij\rangle}\langle f^\dagger_{i\sigma}f_{j\sigma}\rangle^2, \tag{7}$$

where

$$t'=-J_H\langle f^\dagger_{i\sigma}f_{j\sigma}\rangle. \tag{8}$$

Second, we make the approximation of Refs. 10 and 11 to treat the intersite part of the Hamiltonian $\mathcal{H}_1+\mathcal{H}'_2$. By grouping the lattice Green functions in matrix form

$$\boldsymbol{G}_{ij}(\omega)=\begin{pmatrix}G^{dd}_{ij}(\omega) & G^{df}_{ij}(\omega)\\ G^{fd}_{ij}(\omega) & G^{ff}_{ij}(\omega)\end{pmatrix}, \tag{9}$$

and defining the hopping matrices

$$\boldsymbol{T}_{ij}=\begin{cases}\boldsymbol{T}=\begin{pmatrix}t & 0\\ 0 & t'\end{pmatrix} & \text{for } i,j \text{ nearest neighbors},\\ 0 & \text{otherwise},\end{cases} \tag{10}$$

we obtain the following Dyson-like equation:

$$\boldsymbol{G}_{ij}(\omega)=\boldsymbol{g}(\omega)\,\delta_{ij}-\boldsymbol{g}(\omega)\sum_k\,\boldsymbol{T}_{ik}\boldsymbol{G}_{kj}(\omega). \tag{11}$$

The matrix elements of $\boldsymbol{g}_\sigma(\omega)$ are the atomic Green functions at zero temperature which have the form

$$g_{ab}(\omega)=\sum_{i=1}^{4}\frac{A_i}{\omega-p_i}. \tag{12}$$

The poles p_i and the residues A_i are determined from the eigenvalues and eigenvectors of $\mathcal{H}_0$ which are given in Table I of Ref. 10. In a brief preliminary account of this work,[13] we have included in the unperturbed Green functions all the temperature excitations present in the exact atomic solution of the Hamiltonian. In the present version of the approximation, the lattice Green functions are built from the zero temperature atomic Green functions, and their temperature dependence will be described uniquely via the Matsubara frequencies. We have also improved the numerical precision to allow for the computation of the specific heat.

Equation (11) can be solved by Fourier transformation

$$\boldsymbol{G}(\mathbf{q},\omega)=[\mathbf{1}-\boldsymbol{g}(\omega)\boldsymbol{E}(\mathbf{q})]^{-1}\boldsymbol{g}(\omega), \tag{13}$$

where

$$\boldsymbol{E}(\mathbf{q})=-\frac{1}{N}\sum_{ij}\,\boldsymbol{T}_{ij}e^{i\mathbf{q}\cdot(\mathbf{R}_i-\mathbf{R}_j)}=\varepsilon(\mathbf{q})\boldsymbol{T}/t. \tag{14}$$

The matrix elements are

$$G_{dd}(\mathbf{q},\omega)=\frac{g_{dd}(\omega)+t'\,\gamma(\omega)\varepsilon(\mathbf{q})/t}{\Delta(\mathbf{q},\omega)}, \tag{15}$$

$$G_{ff}(\mathbf{q},\omega)=\frac{g_{ff}+\gamma(\omega)\varepsilon(\mathbf{q})}{\Delta(\mathbf{q},\omega)}, \tag{16}$$

$$G_{df}(\mathbf{q},\omega)=\frac{g_{df}}{\Delta(\mathbf{q},\omega)}, \tag{17}$$

where

$$\gamma(\omega)=g^2_{df}(\omega)-g_{dd}(\omega)g_{ff}(\omega), \tag{18}$$

$$\Delta(\mathbf{q},\omega)=1-A(\omega)\varepsilon(\mathbf{q})/t-B(\omega)[\varepsilon(\mathbf{q})/t]^2, \quad (19)$$

$$A(\omega)=tg_{dd}(\omega)+t'g_{ff}(\omega), \quad (20)$$

$$B(\omega)=tt'\gamma(\omega). \quad (21)$$

The lattice Green functions are obtained from the inverse Fourier transformation

$$\boldsymbol{G}_{ij}(\omega)=\frac{1}{N}\sum_{\mathbf{q}}\boldsymbol{G}(\mathbf{q},\omega)e^{-i\mathbf{q}\cdot(\mathbf{R}_i-\mathbf{R}_j)}. \quad (22)$$

For $i=j$ they can be calculated as

$$G_{ii}(\omega)=\frac{1}{N}\sum_{\mathbf{q}}G(\mathbf{q},\omega)=\frac{1}{N}\sum_{\mathbf{q}}F[\varepsilon(\mathbf{q})/t]$$

$$=\int dx\,\rho_0(x)F(x), \quad (23)$$

where $\rho_0(x)$ is the tight-binding density of states of the simple cubic lattice. For the nearest-neighbor Green functions, the corresponding expression is

$$G_{\langle ij\rangle}(\omega)=\frac{1}{N}\sum_{\mathbf{q}}G(\mathbf{q},\omega)e^{iq_xa}=-\frac{1}{6}\int dx\,\rho_0(x)F(x)x. \quad (24)$$

As the kernel function above has the general form

$$F(x)=\frac{C+Dx}{1-Ax-Bx^2}, \quad (25)$$

with C and D defined from Eqs. (15)–(17), the different Green functions can be expressed in terms of the integral transform

$$H(z)=\int dx\frac{\rho_0(x)}{x-z}. \quad (26)$$

Thus, for the general case $J_H\neq 0$ we obtain

$$G_{ii}^{ab}(\omega)=K_+H(Z_+)-K_-H(Z_-), \quad (27)$$

$$G_{\langle ij\rangle}^{ab}(\omega)=\frac{1}{6}\{Z_-K_-H(Z_-)-Z_+K_+H(Z_+)\}, \quad (28)$$

where

$$Z_\pm=-\frac{A\pm\sqrt{A^2+4B}}{2B}, \quad (29)$$

$$K_\pm=\frac{C+DZ_\pm}{B(Z_--Z_+)}. \quad (30)$$

The solution for the particular case $J_H=0$ is

$$G_{ii}^{ab}(\omega)=-\frac{D}{A}-\frac{1}{A}\left(C+\frac{D}{A}\right)H\left(\frac{1}{A}\right), \quad (31)$$

$$G_{\langle ij\rangle}^{ab}(\omega)=-\frac{1}{A}\left(C+\frac{D}{A}\right)\left\{1+\frac{1}{A}H\left(\frac{1}{A}\right)\right\}. \quad (32)$$

The two-operator averages of the model are directly evaluated as a sum over Matsubara frequencies $\omega_n=(2n+1)\pi/\beta$:

$$\langle b_{j\sigma}^\dagger a_{i\sigma}\rangle=\lim_{\tau\to 0^-}\frac{1}{\beta}\sum_n\mathbf{G}_{ij}^{ab}(i\omega_n)e^{i\omega_n\tau}. \quad (33)$$

At low temperatures the asymptotic part of the series has to be evaluated as an integral, by considering ω_n as a continuous variable. The average $\langle f_{i\sigma}^\dagger f_{j\sigma}\rangle$ appearing in Eq. (8) defines a self-consistent evaluation of the lattice Green functions, which always converges, provided that J_H is negative.

The specific heat can be calculated directly from the derivative of the internal energy

$$C=\frac{dE}{dT}. \quad (34)$$

The internal energy per site is given by

$$E=\langle d_{i\sigma}^\dagger[d_{i\sigma},\mathcal{H}]\rangle+\langle f_{i\sigma}^\dagger[f_{i\sigma},\mathcal{H}]\rangle+2V\langle d_{i\sigma}^\dagger f_{i\sigma}\rangle$$

$$-6t\langle d_{i\sigma}^\dagger d_{j\sigma}\rangle-6t'\langle f_{i\sigma}^\dagger f_{j\sigma}\rangle-3J_H\langle f_{i\sigma}^\dagger f_{j\sigma}\rangle^2+\frac{1}{2}E_fn_f, \quad (35)$$

where n_f is the f-electron concentration. The first two terms are calculated by

$$\langle a_{i\sigma}^\dagger[a_{i\sigma},\mathcal{H}]\rangle=\lim_{\tau\to 0^-}\frac{1}{\beta}\sum_n[i\omega_n\mathbf{G}_{ij}^{aa}(i\omega_n)-1]e^{i\omega_n\tau}. \quad (36)$$

In the next section, we will present first the averages $\langle d_{i\sigma}^\dagger f_{i\sigma}\rangle$ and $\langle f_{i\sigma}^\dagger f_{j\sigma}\rangle$ for different values of the parameters. Within the approximation that we have adopted here, these two averages provide a good account for the intrasite d-f correlation and the intersite f-f correlation functions. Finally, Eqs. (34)–(36) will give the specific heat curves versus temperature for the same values of the parameters.

III. RESULTS

First of all, we plot in Fig. 1 the averages $\langle d_{i\sigma}^\dagger f_{i\sigma}\rangle$ and $\langle f_{i\sigma}^\dagger f_{j\sigma}\rangle$ (where i and j are nearest neighbors) as a function of temperature for different values of the parameters E_f, V, and J_H. We choose $E_f=-3t$ and $V=t$. For these values of the parameters, the Anderson Hamiltonian is equivalent to a Kondo exchange Hamiltonian with $J_K=-4t/3$, which is much smaller than the width $W=12t$ of the conduction band. We take several values of $J_H=0,-3t,-6t$, and $-12t$ in order to study the effect of antiferromagnetic intersite correlations. Each curve is a smooth and monotonically increasing function whose derivative exhibits a well marked maximum, which corresponds to a kind of crossover temperature. We define the Kondo temperature T_K as the crossover temperature determined from the average $\langle d_{i\sigma}^\dagger f_{i\sigma}\rangle$. The correlation temperature $T_{\rm cor}$, below which short-range magnetic correlations arise, is defined in a similar way with respect to $\langle f_{i\sigma}^\dagger f_{j\sigma}\rangle$. More precisely, T_K and $T_{\rm cor}$ are taken here equal to the temperatures of the maxima of the derivatives of the curves of Fig. 1 with respect to temperature. From the curves

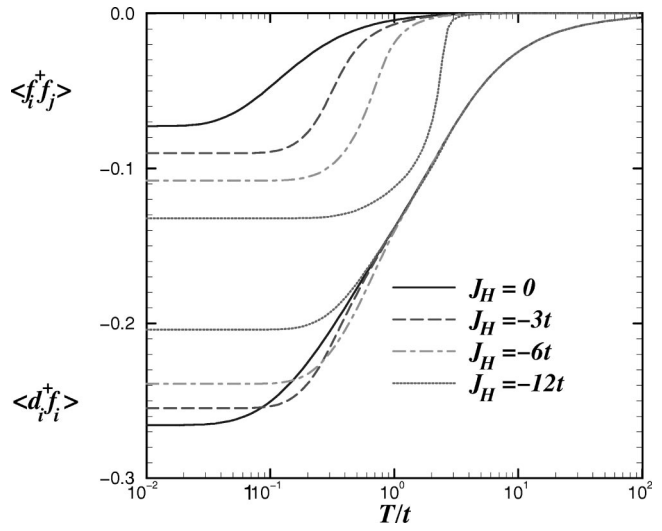

FIG. 1. The averages $\langle d^\dagger_{i\sigma} f_{i\sigma}\rangle$ (lower curves) and $\langle f^\dagger_{i\sigma} f_{j\sigma}\rangle$ (upper curves) as a function of temperature for $E_f=-3t$, $V=t$, and different values of J_H.

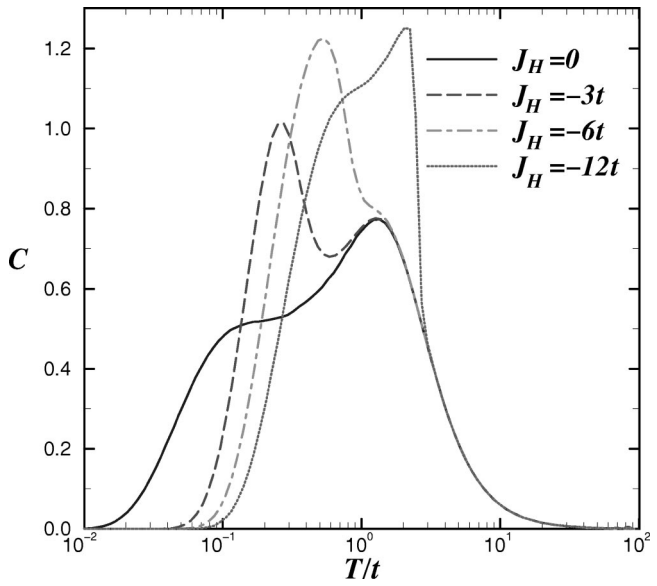

FIG. 3. Specific heat as a function of temperature for the same parameters as in Fig.1.

in Fig. 1, one can remark that $T_{\rm cor}$ increases rapidly with $|J_H|$, while T_K seems to saturate to a constant value. Here, in contrast with the preceding Kondo lattice treatment in Ref. 3, the curves giving $\langle d^\dagger_{i\sigma} f_{i\sigma}\rangle$ and $\langle f^\dagger_{i\sigma} f_{j\sigma}\rangle$ do not present any phase transition but are rather smooth. This indicates that the corresponding definition of T_K provides an improved description of the Kondo effect.

Figure 2 gives a plot of the two temperatures T_K and $T_{\rm cor}$ versus the intersite antiferromagnetic correlation parameter J_H for $V=t$ and $E_f=-3t$. We see that there is a crossing between the two curves at a value $|J_H|\approx 2.57t$ and that the Kondo temperature T_K remains roughly constant, while the short-range correlation temperature $T_{\rm cor}$ increases very rapidly with $|J_H|$.

Figure 3 shows the temperature dependence of the specific heat for the same values of the parameters as those used in Fig. 1. The specific heat curves show a clear peak near $T_{\rm cor}$ and another one at $T\approx t$. As expected, the low temperature peak increases with $|J_H|$, approaches first the high-temperature peak and becomes even larger for the highest value $|J_H|=12t$.

So far, we have studied T_K and $T_{\rm cor}$ as a function of J_H for constant E_f/t and V/t values. The corresponding value of the d-f exchange parameter J_K has also been considered as a constant. In particular, the adopted value $|J_K|=4t/3$ is quite small. Thus, it is interesting to deduce the diagram of T_K and $T_{\rm cor}$ as a function of $|J_K|$, to see what happens when this parameter increases. As previously established for the Kondo lattice,[3] in cerium compounds, the intersite Heisenberg exchange between localized spins originates mainly from the RKKY interaction which is mediated by the conduction electrons via the hybridization. In Ref. 3, J_H/t has been taken

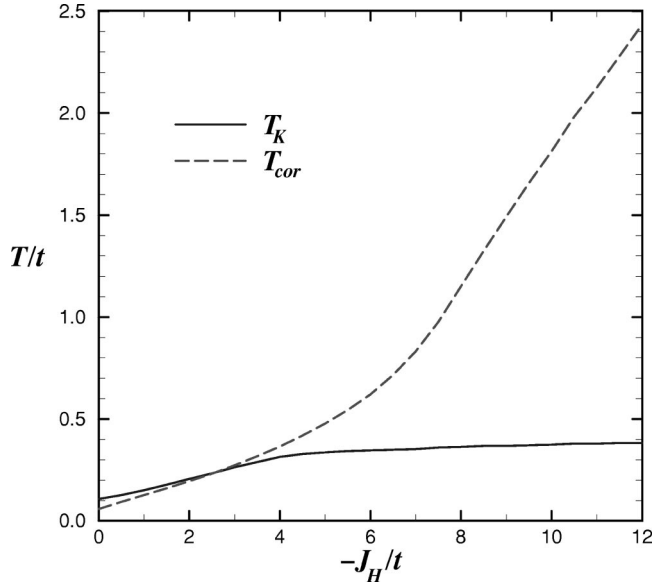

FIG. 2. Crossover temperatures T_K and $T_{\rm cor}$ as a function of J_H/t for $V=t$ and $E_f=-3t$.

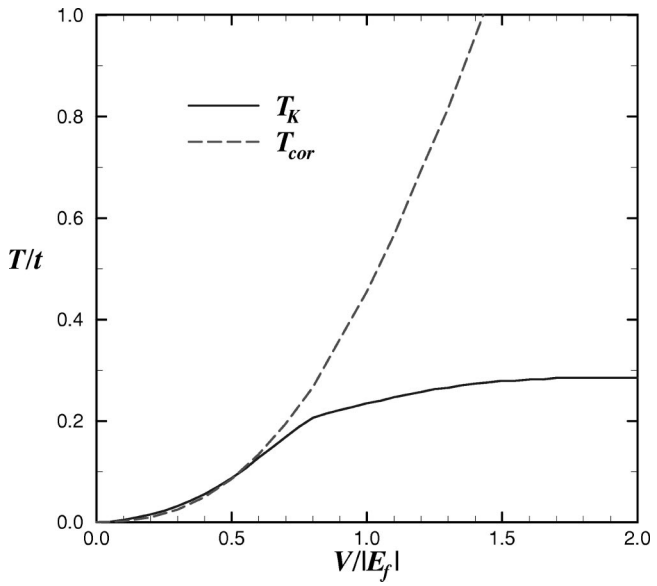

FIG. 4. Crossover temperatures T_K and $T_{\rm cor}$ as a function of the ratio $|V/E_f|$ for $V=0.5t$ and J_H given by Eq. (38).

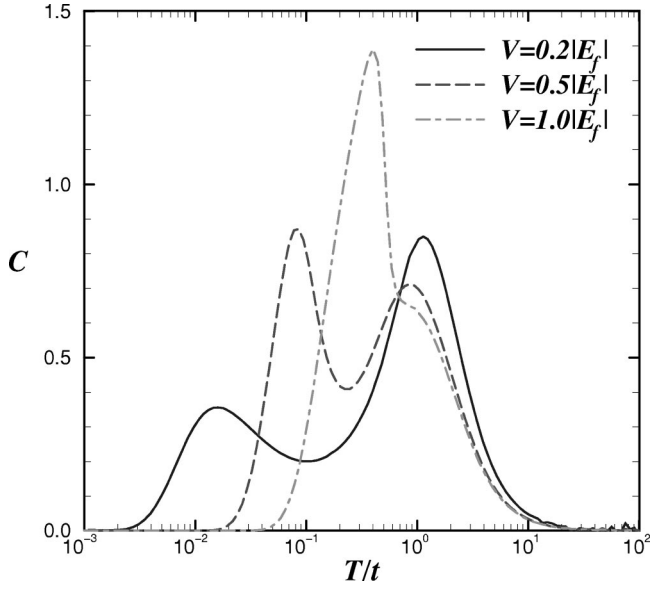

FIG. 5. Specific heat for $V=0.5t$, J_H given by Eq. (38) and different values of $|V/E_f|$.

proportional to $(J_K/t)^2$. We take here the same relation between J_H and the J_K value given by the Schrieffer-Wolff transformation.[12] We obtain a good description of the physical situation of Cerium Kondo compounds if we choose here

$$\frac{J_H}{t} = -0.5\left(\frac{J_K}{t}\right)^2 \tag{37}$$

or, equivalently, by using Eq. (1),

$$\frac{J_H}{t} = -\frac{8V^4}{(E_f t)^2}. \tag{38}$$

Figure 4 shows the plot of the two crossover temperatures T_K and $T_{\rm cor}$ versus $|V/E_f|$ for $V=0.5t$ and J_H given by Eq. (38). We see that $T_{\rm cor}$ increases rapidly and T_K remains roughly constant versus $|V/E_f|$ above a value roughly equal to 1, which corresponds to $J_K=J_H\approx -2t$, which is much smaller than the width $W=12t$ of the conduction band. Thus, Fig. 4 represents the diagram giving T_K and $T_{\rm cor}$ within the periodic Anderson Hamiltonian and the parameter $|V/E_f|$ is expected to be proportional to the pressure.

Finally, we show in Fig. 5 the specific heat for the same parameters as those in Fig. 4 and for different values of $V/|E_f|$. We see that there are also two peaks, the first one corresponding to $T_{\rm cor}$ and the second one to roughly t.

IV. CONCLUDING REMARKS

The present approach provides a phase diagram for the Anderson lattice described by both the Anderson Hamiltonian and an additional Heisenberg-type exchange interaction between the $4f$ spins on nearest neighbors. The calculation has been performed here in the nonmagnetic case, as previously for the Kondo lattice.[3] The magnetic phases of the Anderson lattice have been recently studied through a related approximation developed in Ref. 14.

The present treatment of the Anderson lattice is similar to the ''revisited'' Doniach diagram for the Kondo lattice[3] and gives both the Kondo temperature T_K and the short-range correlation temperature $T_{\rm cor}$. The Kondo temperature increases firstly and then remains constant as a function of $|J_H|$ in Fig. 2 or $|V/E_f|$ in Fig. 4. Thus, this result gives also a revisited version of the Doniach diagram and shows that T_K remains roughly constant with $|V/E_f|$ or $|J_K|$ and then under pressure in the nonmagnetic region above the quantum critical point where the Néel temperature T_N disappears. Our calculation can also account for the occurrence of antiferromagneticlike short-range correlations in some Cerium compounds at a temperature $T_{\rm cor}$ much larger than T_K, such as in $CeRu_2Si_2$ where $T_{\rm cor}\approx 60$–70 K and $T_K\approx 14$–23 K (Refs. 7 and 15) and in $CeCu_6$ where $T_{\rm cor}\approx 10$ K and $T_K\approx 5$ K.[15]

We obtain two improvements with respect to the preceding Kondo lattice mean-field calculation[3]: The curves giving $\langle d^\dagger_{i\sigma} f_{i\sigma}\rangle$ and $\langle f^\dagger_{i\sigma} f_{j\sigma}\rangle$ are smooth and do not present any phase transition, implying that T_K and $T_{\rm cor}$ correspond to crossover temperatures. This point is well known for the Kondo effect, and it has also been established for $T_{\rm cor}$ by neutron scattering experiments.[15] The values obtained here for T_K and $T_{\rm cor}$ are smaller, and consequently in better agreement with the experimental values. As shown in Figs. 2 and 4, T_K/t is typically of order 0.3–0.4 and, since the conduction bandwidth is $W=12t$, T_K is much smaller here than in Ref. 3.

We have also derived the specific heat C which exhibits two maxima at temperatures roughly equal to $T_{\rm cor}$ and t. Further experiments would be interesting to check this form of the specific heat curves. Finally, the inclusion of the extra intersite exchange term in the nonmagnetic phase is necessary to obtain a good description of cerium Kondo compounds and further theoretical work will be still important to better understand this point.

ACKNOWLEDGMENT

We aknowledge the support of the Brazil-France cooperation agreement Capes-Cofecub, Project No. 196/96.

*On leave from Universidade do Estado de Santa Catarina, Joinville, Brazil.

[1] B. Coqblin, J. Arispe, J.R. Iglesias, C. Lacroix, and K. Le Hur, J. Phys. Soc. Jpn. **65**, Suppl. B, 64 (1996).
[2] S. Doniach, Physica B **91**, 231 (1977).
[3] J.R. Iglesias, C. Lacroix, and B. Coqblin, Phys. Rev. B **56**, 11 820 (1997).
[4] T. Graf, J.D. Thompson, M.F. Hundley, R. Movskovich, Z. Fisk, D. Mandrus, R.A. Fisher, and N.E. Phillips, Phys. Rev. Lett. **78**, 3769 (1997).
[5] H. Wilhelm, K. Alami-Yadri, B. Revaz, and D. Jaccard, Phys. Rev. B **59**, 3651 (1999).
[6] S. Sullow, M.C. Aronson, B.D. Rainford, and P. Haen, Phys. Rev. Lett. **82**, 2963 (1999).
[7] J. Flouquet, S. Kambe, L.P. Regnault, P. Haen, J.P. Brison, F. Lapierre, and P. Lejay, Physica B **215**, 77 (1995).
[8] Y. Miyako, T. Takeuchi, T. Taniguchi, S. Kawarazaki, K. Marumoto, R. Hamada, Y. Yamamoto, M. Ocio, P. Pari, and J. Hammann, J. Phys. Soc. Jpn. **65**, Suppl. B, 12 (1996).
[9] Ph. Nozières, Eur. Phys. J. B **6**, 447 (1999).

[10] L.G. Brunet, M.A. Gusmão, and J.R. Iglesias, Phys. Rev. B **46**, 4520 (1992).
[11] B.H. Bernhard and J.R. Iglesias, Phys. Rev. B **47**, 12 408 (1993).
[12] J.P. Schrieffer and P.A. Wolff, Phys. Rev. **149**, 491 (1966).
[13] B.H. Bernhard, C. Lacroix, J.R. Iglesias, and B. Coqblin, Physica B **259-261**, 227 (1999).
[14] B.H. Bernhard and C. Lacroix, Phys. Rev. B **60**, 12149 (1999).
[15] J. Rossat-Mignod, L.P. Regnault, J.L. Jacoud, C. Vettier, P. Lejay, J. Flouquet, E. Walker, D. Jaccard, and A. Amato, J. Magn. Magn. Mater. **76-77**, 376 (1988).